

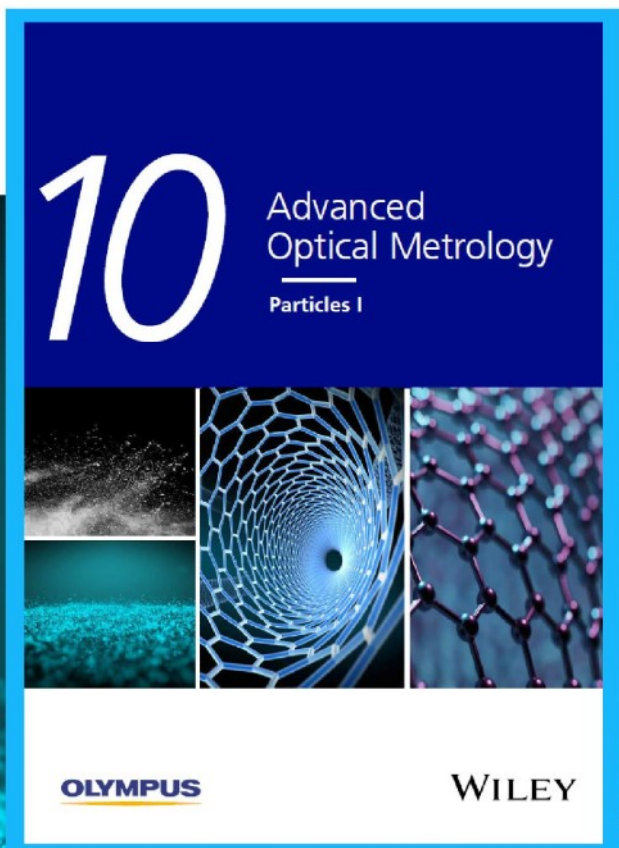


Particles I

Access the latest eBook →

Particles: Unique Properties,
Uncountable Applications

**Read the latest eBook and
better your knowledge with
highlights from the recent
studies on the design and
characterization of micro-
and nanoparticles for
different application areas.**



Access Now

This eBook is sponsored by

OLYMPUS

WILEY

Thermal Conductivity of HfTe₅: A Critical Revisit

Tianli Feng, Xuewang Wu, Xiaolong Yang, Peipei Wang, Liyuan Zhang, Xu Du, Xiaojia Wang,* and Sokrates T. Pantelides*

Hafnium pentatelluride (HfTe₅) has attracted extensive interest due to its exotic electronic, optical, and thermal properties. As a highly anisotropic crystal (layered structure with in-plane chains), it has highly anisotropic electrical-transport properties, but the anisotropy of its thermal-transport properties has not been established. Here, accurate experimental measurements and theoretical calculations are combined to resolve this issue. Time-domain thermoreflectance measurements find a highly anisotropic thermal conductivity, 28:1:8, with values of 11.3 ± 2.2 , 0.41 ± 0.04 , and 3.2 ± 2.0 W m⁻¹ K⁻¹ along the in-plane *a*-axis, through-plane *b*-axis, and in-plane *c*-axis, respectively. This anisotropy is even larger than what was recently established for ZrTe₅ (12:1:6), but the individual values are somewhat higher, even though Zr has a smaller atomic mass than Hf. Density-functional-theory calculations predict thermal conductivities in good agreement with the experimental data, provide comprehensive insights into the results, and reveal the origin of the apparent anomaly of the relative thermal conductivities of the two pentatellurides. These results establish that HfTe₅ and ZrTe₅, and by implication their alloys, have highly anisotropic and ultralow through-plane thermal conductivities, which can provide guidance for the design of materials for new directional-heat-management applications and potentially other thermal functionalities.

to a structural phase transition,^[1,2] formation of a charge/spin density wave,^[1,3,4] polaronic behavior,^[5] bipolar conduction,^[6] etc.^[7,8] Recently, interest in ZrTe₅ and HfTe₅ was boosted by the discovery of extraordinary topological properties^[9–16] and the promise of potential thermoelectric applications.^[17,18] Even more recently, rather exotic thermal-transport properties were found in single-crystalline ZrTe₅.^[19] The through-plane lattice thermal conductivity κ_L was found to be 0.33 W m⁻¹ K⁻¹ at room temperature, which is lower than the lowest reported room-temperature κ_L value among bulk crystalline thermoelectric materials (0.47 W m⁻¹ K⁻¹ for SnSe^[20]). Given that HfTe₅ has the same lattice structure as ZrTe₅ with even heavier atomic mass, it is intuitive to hypothesize that HfTe₅ might have similar or even lower κ_L , promising the possibility of ultralow thermal conductivity for applications in thermal barrier coatings, thermal management, and thermoelectrics.

So far, very little is known about the thermal conductivity of single-crystalline HfTe₅. In 2000, experimental values rising from 4.5 W m⁻¹ K⁻¹ at room temperature to about 13.5 W m⁻¹ K⁻¹ at 20 K and then dropping to 10 W m⁻¹ K⁻¹ at 10 K were reported.^[21] The reliability of these data was questioned recently, however, because of difficulties in measurements using needle-shaped samples.^[17] No directionally resolved data have been reported. Density-functional-theory

1. Introduction

Transition-metal pentatellurides, such as ZrTe₅ and HfTe₅, have drawn extensive attention since the late 1970's due to their mysterious resistivity anomalies^[1,2]—the resistivity exhibits a peak and the Seebeck coefficient changes sign. The underlying mechanism has been the subject of debate, attributed variously

Dr. T. Feng, Prof. S. T. Pantelides
Department of Physics and Astronomy and Department of Electrical Engineering and Computer Science
Vanderbilt University
Nashville, TN 37235, USA
E-mail: pantelides@vanderbilt.edu

Dr. T. Feng, Prof. S. T. Pantelides
Materials Science and Technology Division
Oak Ridge National Laboratory
Oak Ridge, TN 37831, USA

Dr. X. Wu, Prof. X. Wang
Department of Mechanical Engineering
University of Minnesota
Minneapolis, MN 55455, USA
E-mail: wang4940@umn.edu

 The ORCID identification number(s) for the author(s) of this article can be found under <https://doi.org/10.1002/adfm.201907286>.

Dr. X. Yang
Frontier Institute of Science and Technology, and State Key Laboratory for Mechanical Behavior of Materials
Xi'an Jiaotong University
Xi'an 710049, China

Dr. P. Wang, Prof. L. Zhang
Department of Physics
Southern University of Science and Technology, and Shenzhen Institute for Quantum Science and Engineering
Shenzhen 518055, China

Prof. X. Du
Department of Physics and Astronomy
Stony Brook University
Stony Brook, NY 11794, USA

Prof. X. Wang
Department of Electrical and Computer Engineering
University of Minnesota
Minneapolis, MN 55455, USA

DOI: 10.1002/adfm.201907286

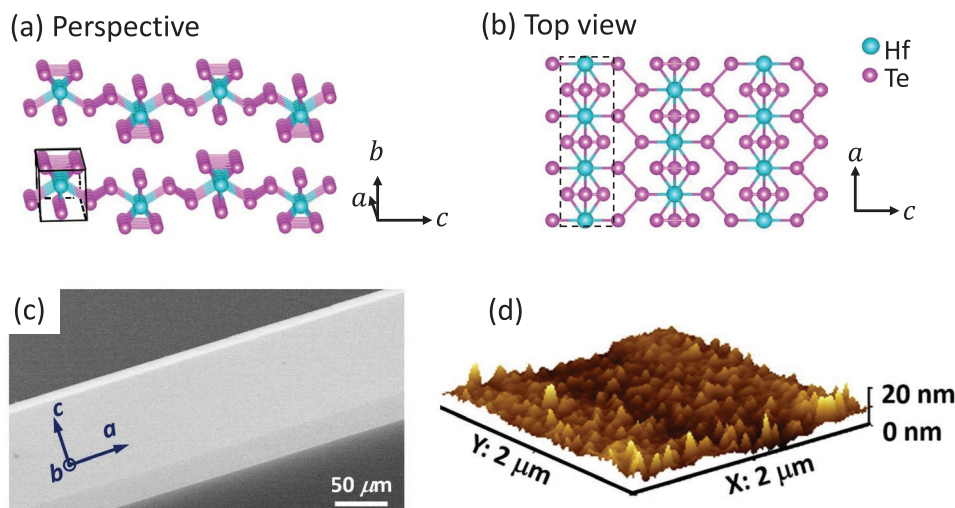


Figure 1. a) Perspective and b) top view of the crystal structure of HfTe₅. The boxes indicate 1D HfTe₃ prism chain. c) SEM image of the HfTe₅ sample. The *a*-axis is along the long edge of the needle-like single crystal. The scale bar is 50 μm. d) AFM image of the sample topology (scanned over a 2 μm × 2 μm area). The RMS roughness is 2.4 nm.

(DFT)-based calculations of the thermal conductivity of HfTe₅ were reported recently.^[22] A directionally averaged room-temperature value of 5.51 W m⁻¹ K⁻¹ was derived, which is close to the experimental value of ref. [21]. However, the calculated directionally resolved values revealed only a small degree of anisotropy, 1.65:1.16:1. Both the large values and the virtual absence of anisotropy are surprising in view of the much smaller and highly anisotropic experimental and theoretical values recently reported for ZrTe₅.^[19] We note, however, that the calculations of ref. [22] included van der Waals (vdW) interactions, which is a practice with at best a mixed record in producing results in agreement with experimental data,^[23] with the weight of the evidence^[23] in favor of omitting vdW interactions. Prior studies of the thermal transport of vdW crystals including multilayer graphene, graphite, and Bi₂Te₃ have shown the standard DFT could agree well (or even better) with experimental data,^[24–26] when the vdW functional was excluded. Thus, the recently reported excellent agreement between theory and experimental data for the thermal conductivities of ZrTe₅, for which the DFT calculations eschewed vdW interactions,^[19] leaves the question of the thermal conductivities of HfTe₅ wide open.

In this paper, we address the open question of the lattice thermal conductivity of HfTe₅ by combining experimental measurements and theoretical calculations, which are in excellent agreement with each other. On the experimental side, we synthesize bulk single-crystal HfTe₅ and measure its thermal conductivity along the three primary crystalline directions using the time-domain thermoreflectance (TDTR) and beam-offset methods. On the theoretical side, we employ DFT calculations without vdW interactions, as in ref. [19], with solutions of the phonon Boltzmann transport equation (BTE) beyond the relaxation-time approximation. We also examine the possible effect of four-phonon scattering, as extensively discussed recently.^[27–29] The thermal conductivities of HfTe₅ are found to have an even higher anisotropy than those of ZrTe₅, but the individual values are somewhat larger even though Zr has a smaller atomic

mass than Hf and ZrTe₅ has larger phonon group velocities. Using density-functional-theory calculations, we identify the origin of this apparent anomaly to be longer acoustic-phonon relaxation times, resulting from a weaker anharmonicity. The weaker anharmonicity is also responsible for a smaller phonon-dispersion renormalization effect for HfTe₅ compared with ZrTe₅ at finite temperatures. The theoretical results are analyzed from several spectral perspectives, including phonon frequency, velocity, specific heat, and mean free path (MFP).

2. Results and Discussion

HfTe₅ has a quasi-1D layered structure as shown in **Figure 1a,b**: Each 2D layer in the *a*-*c* plane contains *a*-oriented HfTe₃ prismatic chains. The layers are stacked along the *b*-axis to form the bulk phase. **Figure 1c** shows a scanning electron microscopy (SEM) image of HfTe₅ surface, which is a good representative of the needle-like shape of the HfTe₅ crystal (resulting from its quasi-1D layered structure) and also its good surface quality. Additional atomic force microscopy (AFM) measurement is carried out to more accurately quantify the surface smoothness. We find that the root mean square (RMS) roughness is only 2.4 nm for a 2 μm × 2 μm area, as shown in **Figure 1d**.

The through-plane and in-plane thermal conductivities of HfTe₅ are measured using TDTR and the beam-offset method. Details have been described in previous papers.^[30–33] **Figure 2** shows the representative TDTR signals and fitting curves at three modulation frequencies. Surprisingly, we find that the through-plane (along the *b*-axis) thermal conductivity of HfTe₅ is 0.41 ± 0.04 W m⁻¹ K⁻¹, which is ≈25% larger than 0.33 ± 0.03 W m⁻¹ K⁻¹ for ZrTe₅.^[19] This result is in sharp contrast with the sole prior data sole theory for the two materials,^[21,22] both of which found much larger average values, with the ZrTe₅ values about 40–50 times larger. Though our result for HfTe₅ is of the same order of magnitude of the established value of ZrTe₅, as it should be because the two materials

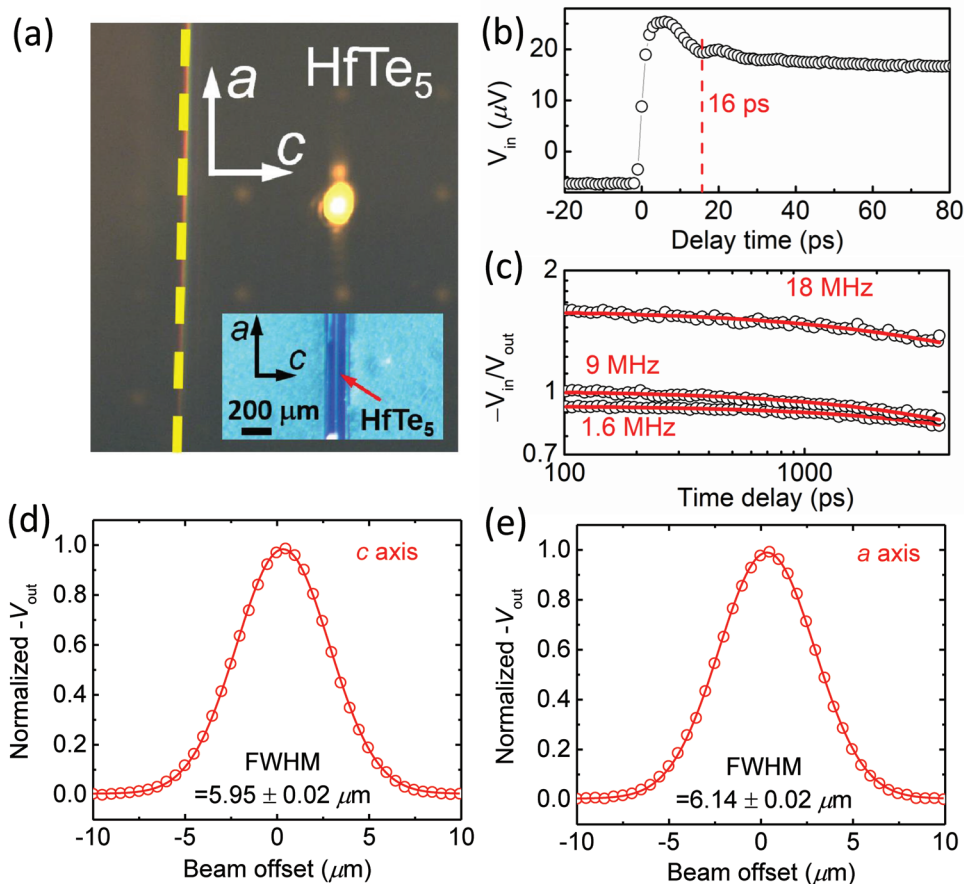


Figure 2. Through-plane and in-plane thermal conductivity measurements. a) Representative CCD image of the HfTe₅ sample illuminated with a laser beam spot of $\approx 2.8 \mu\text{m}$ ($20\times$ objective lens). The a -axis is along the vertical direction and the dashed yellow line represents the long edge of the needle-like HfTe₅ crystal. The inset is a lower-magnification optical microscopic image illustrating the needle-like shape and the sample loading orientation of the single-crystal HfTe₅. The scale bar in the inset is $200 \mu\text{m}$. b) The TDTR V_{in} signals for determining the Al thickness through picosecond acoustics. The first echo at 16 ps indicates an Al thickness of 51 nm ; c) TDTR ratio ($-V_{\text{in}}/V_{\text{out}}$) signals (open circles) at $f_m = 18, 9,$ and 1.6 MHz with the corresponding best-fit curves (red solid lines). d, e) The beam-offset signals along the c and a axes, respectively.

have the same structure, our result is counterintuitive since the atomic mass of Hf is heavier than Zr, and the phonon velocity of HfTe₅ is lower than ZrTe₅ as indicated in ref. [22]. To ensure that the measured results are reproducible and reliable, we chose eight different locations on different flakes and obtained a variation of less than 5%, smaller than the typical 10% uncertainty of TDTR measurements for through-plane thermal conductivities. The interfacial thermal conductance between the Al film and HfTe₅ from TDTR measurements is within the range of $10\text{--}13 \text{ W m}^{-2} \text{ K}^{-1}$ for all flakes, suggesting a relatively weaker interfacial thermal transport between Al and HfTe₅ than what is typical between a metal and a semiconductor. Such a low level of interfacial thermal conductance is also consistent with that between an Al film and ZrTe₅ ($7\text{--}11 \text{ W m}^{-2} \text{ K}^{-1}$) found in previous work.^[19] Given the reservations expressed in the introduction about the prior experimental and theoretical results, we consider our results reliable and reproducible and continue with our exposition, reporting experimental and theoretical results that will further strengthen this conclusion.

To measure the in-plane thermal conductivities of HfTe₅, we utilize the beam-offset method.^[32,34,35] Figure 2a shows a

charge-coupled device (CCD) image of a flake with a $20\times$ objective lens (beam spot size of $\approx 2.8 \mu\text{m}$), in which the a -axis is along the vertical direction. The thermal conductivity of an Al transducer has a significant effect on the beam-offset signals (see Figure S1 in the Supporting Information for details). Thus, its value needs to be accurately determined to obtain reliable in-plane thermal conductivities of HfTe₅ through the beam-offset method. We follow the same procedures as stated in a previous work^[19] by measuring the thermal conductivity of Al for an Al/SiO₂ reference sample placed next to the HfTe₅ samples during the same Al sputtering deposition. We obtain the thermal conductivity of the Al transducer to be $59 \pm 3 \text{ W m}^{-1} \text{ K}^{-1}$ as averaged over three locations. The in-plane thermal conductivities are obtained by matching the full width at half maximum (FWHM) of V_{out} along the x or y directions with the calculated values from the thermal model.^[34,36] Figure 2d,e shows representative beam-offset signals (normalized to the maximum value) along the c and a axes, respectively. The in-plane thermal conductivities of HfTe₅ are measured to be $\kappa_a = 11.3 \pm 2.2 \text{ W m}^{-1} \text{ K}^{-1}$ and $\kappa_c = 3.2 \pm 2.0 \text{ W m}^{-1} \text{ K}^{-1}$, averaged over six locations. The variations of in-plane thermal conductivities among different

locations are less than 15% and 20% along c and a axes, respectively, which are within the corresponding uncertainties of the in-plane thermal conductivities from the beam-offset method (see Table S2 in the Supporting Information for detailed values of uncertainty at different locations and ref. [32] for the method of determining the corresponding uncertainty in the beam-offset measurement). As is the case for the through-plane thermal conductivity, the in-plane thermal conductivity κ_a of HfTe₅, 11.3 W m⁻¹ K⁻¹ is larger than that of ZrTe₅, which is 4.2 W m⁻¹ K⁻¹ (κ_c for ZrTe₅ could not be measured,^[19] but its calculated value, 1.9 W m⁻¹ K⁻¹ is smaller than that of HfTe₅, namely, 3.2 W m⁻¹ K⁻¹).

To gain insight into the physical origin of the higher thermal conductivities of HfTe₅, we have performed first-principles calculations of the exact solution to the phonon BTE^[37–39]

$$\kappa_{L,\alpha} = \frac{1}{N_{\mathbf{q}} V_{\text{cell}}} \sum_{\mathbf{q}, \mathbf{j}} c_{\mathbf{q}, \mathbf{j}} v_{\mathbf{q}, \mathbf{j}, \alpha}^2 \tau_{\mathbf{q}, \mathbf{j}} \quad (1)$$

in which α denotes the transport directions x , y , and z , (\mathbf{q}, \mathbf{j}) represent a phonon mode with wave vector \mathbf{q} and dispersion branch \mathbf{j} , V_{cell} is the volume of a primitive cell, and $N_{\mathbf{q}}$ is the total number of \mathbf{q} points sampled in the Brillouin zone. The thermal conductivity of each phonon mode is calculated by the product of its specific heat $c_{\mathbf{q}, \mathbf{j}}$, group velocity $v_{\mathbf{q}, \mathbf{j}, \alpha}$, and the relaxation time $\tau_{\mathbf{q}, \mathbf{j}}$. The specific heat per mode is $c_{\mathbf{q}, \mathbf{j}} = \hbar \omega_{\mathbf{q}, \mathbf{j}} \partial n_{\mathbf{q}, \mathbf{j}} / \partial T = k_{\text{B}} x^2 e^x / (e^x - 1)^2$, where $n_{\mathbf{q}, \mathbf{j}}$ is the phonon occupation number that obeys the Bose–Einstein distribution $n_{\mathbf{q}, \mathbf{j}} = (e^x - 1)^{-1}$ with $x = \hbar \omega_{\mathbf{q}, \mathbf{j}} / k_{\text{B}} T$.

The phonon dispersion relation of HfTe₅ is compared to that of ZrTe₅^[19] in **Figure 3**. We find that the ground-state (0 K) calculation features a negative transverse-acoustic branch, which vibrates along the c -axis while it transports along the b -axis, for both materials. This negative energy branch might indicate that the structure has an instability at 0 K in DFT. Via renormalization at finite temperatures^[40] (considering the effect of finite temperature on the phonon frequencies), this negative branch is eliminated without changing the other branches significantly. We find that even at very low temperature, phonon renormalization can eliminate this negative branch. Furthermore, we find that renormalization has a bigger effect on the phonon dispersion of ZrTe₅ than HfTe₅, partially indicating that ZrTe₅ is more anharmonic (softer). Compared to ZrTe₅, HfTe₅ features

lower phonon frequencies due to the heavier atomic mass. However, due to the large stoichiometric ratio of Te in the compounds, the phonon spectra are dominated by Te rather than Hf or Zr atoms. Since the mass of Te is heavy, it dominates mostly the low-frequency phonon spectra. Therefore, it can be found from **Figure 3** that replacing Zr with Hf does not change the acoustic and low-frequency optical phonon spectra (below 3.5 THz) significantly.

The calculated thermal conductivities based on three-phonon scattering along the a , b , and c axes as functions of temperature are shown in **Figure 4a**. The room-temperature κ_a , κ_b , and κ_c are 4.8, 0.47, and 2.4 W m⁻¹ K⁻¹, respectively. We note that the theoretical κ_a and κ_c are significantly smaller than the measured values, namely, 11.3, and 3.2 W m⁻¹ K⁻¹. A possible origin of the discrepancy is that the electronic thermal conductivity contributions are large. To examine this hypothesis, we conducted measurements of electrical resistivity. However, due to the small sizes of HfTe₅ crystals, it was possible to measure the electrical conductivity only along the a -axis. The measured results are shown in **Figure S2** in the Supporting Information. The electrical resistivity measured at 300 K is about 0.14 mΩ cm and the corresponding electronic thermal conductivity is about 5.2 W m⁻¹ K⁻¹, which indeed reasonably compensates the difference between the measured total thermal conductivity, 11.3 W m⁻¹ K⁻¹, and the calculated phonon thermal conductivity, 4.8 W m⁻¹ K⁻¹, along the a -axis, supporting our hypothesis. Such high electronic contribution to the thermal conductivity was not found in ZrTe₅,^[19] which is consistent with the fact that the electrical conductivity of single-crystalline ZrTe₅ is several times lower than that of HfTe₅.^[41] On the other hand, the theoretical through-plane thermal conductivity κ_b is consistent with the experimental value since the through-plane electrical conductivity is quite low.

As can be seen in **Figure 4a,b** and **Table 1**, both the theoretical and experimental lattice thermal conductivities of HfTe₅ are larger than those of ZrTe₅, which goes contrary to the intuitive argument that the larger Hf mass compared with the Zr mass should yield smaller lattice thermal conductivities.

To understand this anomaly, we calculated the cumulative and spectral thermal conductivities as functions of frequency as shown in **Figure 4 c–f** (also see **Figure S2** in the Supporting Information for the branch-resolved thermal conductivity contribution). We find that the difference in κ_L for these two

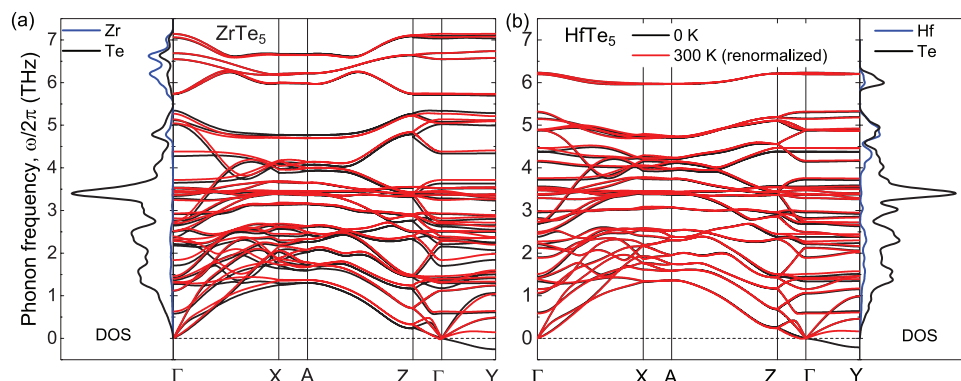


Figure 3. Phonon dispersion relations and density of states of a) ZrTe₅ and b) HfTe₅ calculated using DFT.

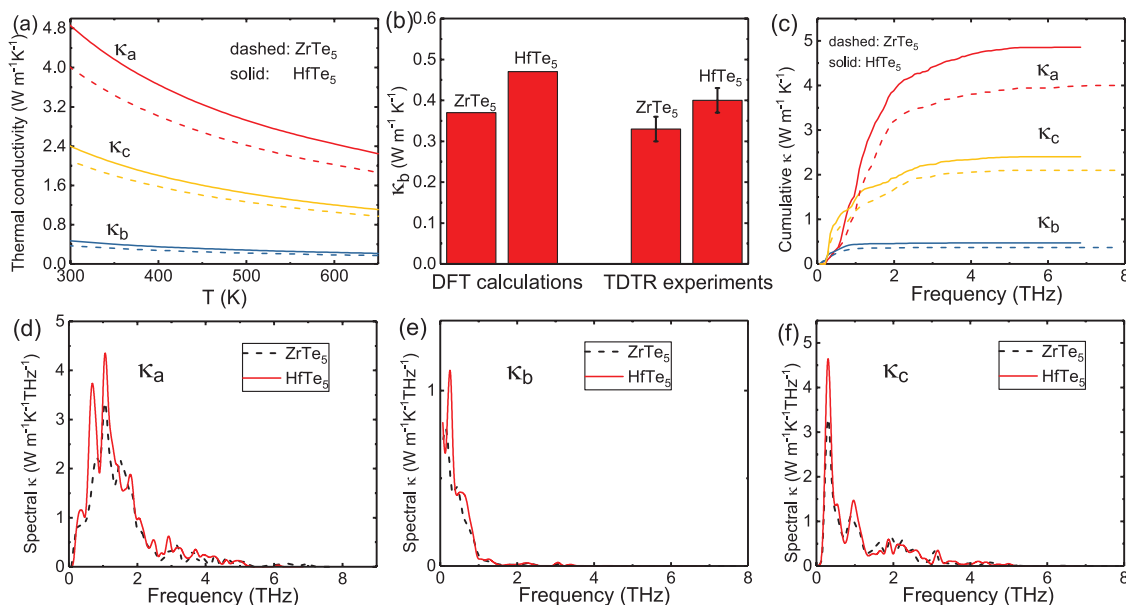


Figure 4. a) The thermal conductivities κ_a , κ_b , and κ_c of ZrTe_5 and HfTe_5 as a function of temperature from DFT calculations including up to three-phonon scattering. b) The through-plane theoretical and experimental thermal conductivities κ_b . c) The cumulative thermal conductivities as a function of phonon frequency. d–f) The spectral thermal conductivities as functions of phonon frequency.

materials mostly comes from phonon branches in the range 0–2 THz while the phonon branches in the range 2–7 THz contribute little to κ_L , even though they have much larger density of states (Figure 3).

To explore the origins of the difference for the low-frequency phonons (below 2 THz), we look into the three factors, phonon group velocity, specific heat, and relaxation times, that determine lattice thermal conductivities. Figure 5a shows the phonon group velocities along a , b , and c axes of HfTe_5 and ZrTe_5 . It is found that HfTe_5 has generally lower group velocities than ZrTe_5 . This is within expectations since Hf atoms are heavier than Zr atoms, and the phonon dispersion shows a softening effect as shown in Figure 3. Therefore, phonon velocities are not the origin of the anomalously higher κ_L of HfTe_5 . We then, turn to the second factor—specific heat. However, HfTe_5 has only slightly higher ($\approx 2\%$) specific heat than ZrTe_5 (see Figures S3 and S4 in the Supporting Information for details). With these two factors excluded, the phonon relaxation time is the only possible factor responsible for the anomaly in the thermal conductivities of the two materials. Indeed, as illustrated in Figure 5a, the phonon relaxation times of HfTe_5 are

larger than those of ZrTe_5 , which is beyond expectation since normally the phonon relaxation time decreases for elements moving downward in the periodic table, as lattice anharmonicity increases.^[27,39]

Once the phonon relaxation time is identified as the main influential factor on the scaling of thermal conductivities, we further examine the two factors that govern phonon relaxation times: the scattering phase space and anharmonicity. We find that the former is not a reason since the narrower phonon frequency spectrum of HfTe_5 allows larger scattering phase space than ZrTe_5 (see Figure S5 in the Supporting Information for details), as also shown by Wang et al.^[22] To investigate the anharmonicity, we calculated the Grüneisen parameters and find them to be 1.22 and 1.23 for HfTe_5 and ZrTe_5 , respectively. The virtually identical Grüneisen parameters cannot cause a substantial change in scattering rates either. However, we notice that the amplitudes of the low-frequency mode-dependent Grüneisen parameters $\gamma_{k,j}$ of HfTe_5 are considerably smaller than those of ZrTe_5 (Figure 6). To quantify the difference between them, we compare the amplitude of the Grüneisen parameter by integrating over the phonon frequency ranging from 0 to 2 THz based on

Table 1. Comparison between the measured and predicted thermal conductivities of HfTe_5 and ZrTe_5 . The units are $\text{Wm}^{-1} \text{K}^{-1}$. The measured data include both lattice and electron contributions while the predicted data only contain the lattice contribution.

		κ_a	κ_b	κ_c
HfTe_5	Experiment	11.3	0.41	3.2
	Theory	4.8	0.47	2.4
ZrTe_5	Experiment	4.2	0.33	–
	Theory	3.9	0.36	1.9

$$|\gamma(\omega)| = \frac{\sum_{\mathbf{k},j}^{\omega} c_{\mathbf{k},j} |\gamma_{\mathbf{k},j}|}{\sum_{\mathbf{k},j} c_{\mathbf{k},j}} \quad (2)$$

Here, we take the absolute values of $\gamma_{k,j}$ to inspect the amplitude of anharmonicity. Equation (2) can recover the total Grüneisen parameter of the material if the absolute operator (“|” sign) in Equation (2) is removed. As shown in the inset, the total Grüneisen parameter of these phonons in HfTe_5 is 20% smaller than that in ZrTe_5 , indicating that HfTe_5 is more

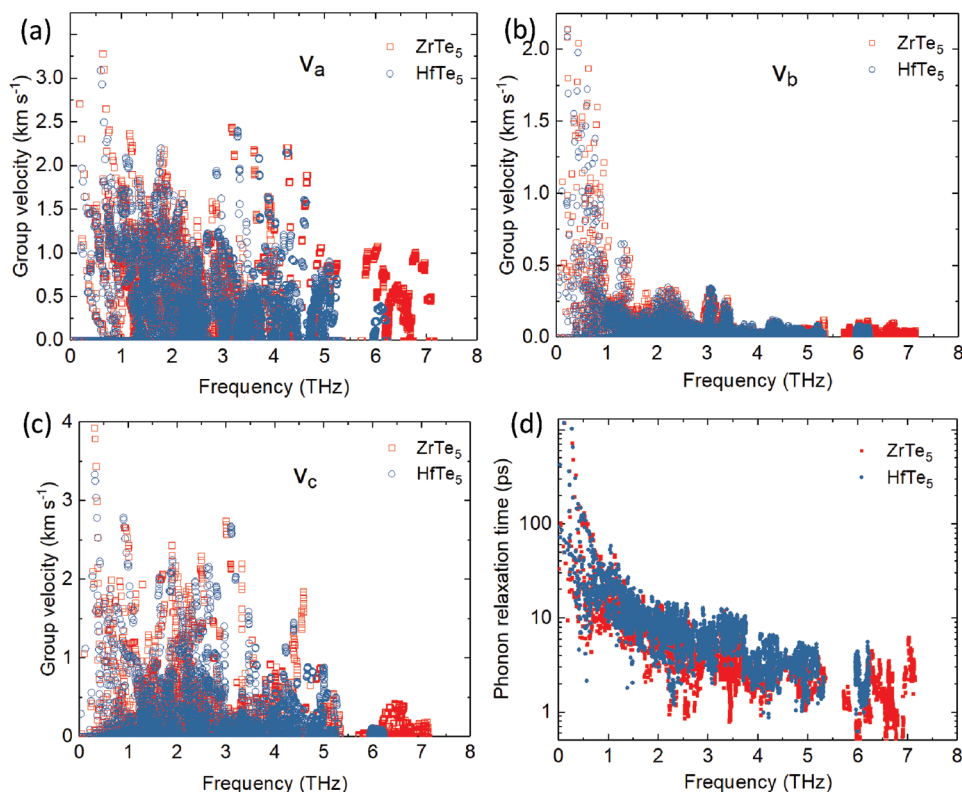


Figure 5. a–c) The phonon group velocities of HfTe₅ and ZrTe₅ along *a*, *b*, and *c* axes. d) Phonon relaxation times of HfTe₅ and ZrTe₅ at room temperature.

harmonic, especially to the acoustic phonons. This finding is consistent with the preceding discussion that the phonon renormalization makes a smaller change to the dispersion of HfTe₅ than to ZrTe₅.

We notice a similar phenomenon, i.e., a heavier material shows weaker anharmonicity, is also found in other

systems.^[42–44] For example, Bi₂Te₃ and Sb₂Te₃ share the same lattice structure and similar lattice constants, and the Grüneisen parameter of Bi₂Te₃ (1.5^[42]) is smaller than that of Sb₂Te₃ (1.7^[42]–2.3^[43]) although Bi is heavier than Sb. Another example is lead chalcogenides,^[44] e.g., PbS, PbSe, and PbTe, with acoustic Grüneisen parameters of 2.50–2.52, 2.23–2.29, and 1.96–2.18, decreasing with increasing atomic mass. But in these systems, an anomalous thermal conductivity is not observed. For example, the heavier materials Bi₂Te₃ do not necessarily have higher thermal conductivity (e.g., than Sb₂Te₃) since the lower group velocity and larger scattering phase space of the former dominates over its smaller anharmonicity. The Grüneisen parameter is also related to the coefficient of thermal expansion (CTE). For example, CTE of Bi₂Te₃ ($5.2 \times 10^{-5} \text{ K}^{-1}$) is considerably smaller than that of Sb₂Te₃ ($7.1 \times 10^{-5} \text{ K}^{-1}$). Therefore, HfTe₅ may have a smaller CTE than ZrTe₅. It should be noted that not all chalcogenides show such an abnormal behavior (e.g., the Grüneisen parameter of Bi₂Se₃ is smaller than Bi₂Te₃).^[43] The underlying physics that governs the anharmonicity is complicated and is still under investigation.^[42,44–47]

We note that most recently it was pointed out that the “phonon gas model” used in the phonon BTE cannot fully account for thermal transport in materials with ultralow thermal conductivity.^[48] The reason is that a large number of phonons in these materials have MFPs that are shorter than the interatomic distance (Ioffe–Regel limit^[49]). Therefore, the phonon gas model fails to account for their contributions to thermal transport, which should be included in other forms such as the Einstein model used in ref. [48]. HfTe₅ and ZrTe₅ have ultralow

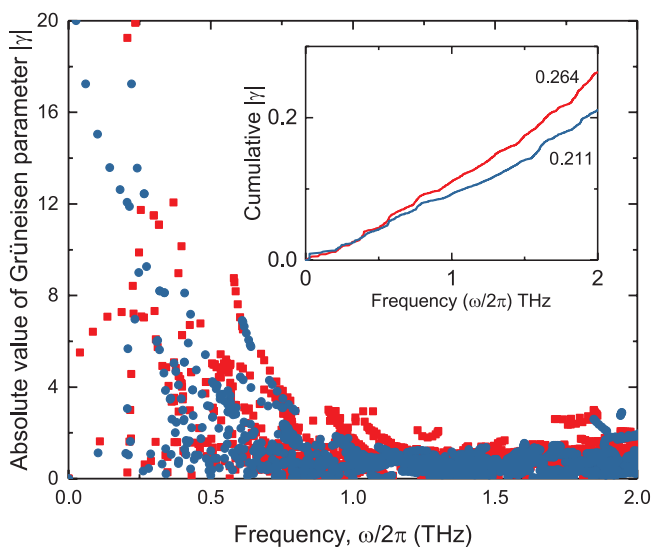


Figure 6. The absolute value of mode-dependent Grüneisen parameters of HfTe₅ and ZrTe₅ from 0 to 2 THz. The inset shows its accumulation as a function of frequency.

thermal conductivities and most of the high-frequency phonons that take more than a half of the total vibrational density of states do not contribute to the total thermal conductivity based on the phonon BTE model. It appears that these phonons may contribute to thermal transport in other forms. However, after inspecting the phonon MFP spectra, we find that most of these phonons are above the Ioffe–Regel limit (see Figure S6 in the Supporting Information for details) and their MFPs are longer than those in other low-thermal-conductivity materials.^[20,48] The reason for their negligible thermal conductivity along the through-plane direction is the phonon focusing effect, i.e., the phonon transport is focused on the in-plane direction, leaving the projection on the through-plane direction to be very small. In other words, although the projection of phonon velocity along the through-plane is small, the total phonon velocity amplitude is large, and therefore it does not hit the Ioffe–Regel limit. Nevertheless, we do not rule out the possibility that the phonons below Ioffe–Regel limit may need further consideration beyond the BTE model for HfTe₅.

An extra caution that needs to be taken for materials with ultralow thermal conductivity is the higher-order phonon scattering.^[27,28] The large unit cell of HfTe₅, however, eliminates the possibility of doing a strict four-phonon scattering calculation. As indicated by Feng and Ruan^[27] and Feng et al.,^[28] four-phonon scattering is important for the thermal transport in materials with strong anharmonicities and materials with acoustic-optical bandgaps or at high temperatures. Fortunately, in our cases, there is no acoustic-optical bandgap, and the ultralow thermal conductivities do not originate from strong anharmonicity (but from the phonon focusing effect instead, as discussed in preceding text). Also, we focus on room temperature, which may not excite strong four-phonon scattering. Nevertheless, the four-phonon scattering in ZrTe₅ and HfTe₅ is still open to study in the future.

Since transition-metal pentatellurides are found to have the lowest through-plane thermal conductivities among the reported single crystals, it is interesting to compare them with other layered materials. In Table 2, we list the through-plane Γ -center (long-wavelength) LA phonon velocities and thermal conductivities of various layered crystals. The group velocities are generally 2–5 km s⁻¹, which are much smaller than those of general covalent materials with similar atomic masses. Black phosphorous and graphite are highest among them since their atomic masses are lightest. The transition metal dichalcogenides (TMDs) show smaller group velocities even than Bi₂Te₃ and SnSe, two state-of-the-art thermoelectric materials, since their interlayer interactions are weaker. Among these materials, HfTe₅ has the lowest through-plane group velocities, which are attributed to the heavy atomic mass as well as weak interlayer interaction. This explains partially their lowest through-plane

thermal conductivities among these materials. It is interesting to note that the TMD materials MoSe₂ and WSe₂ show opposite trends for group velocity and thermal conductivity, similar to the transition-metal pentatellurides ZrTe₅ and HfTe₅.

The large anisotropy of the lattice thermal conductivity endows HfTe₅ with a great potential for new directional-heat-management applications, in which it can act as either a heat spreader or insulator depending on the direction. The low through-plane thermal conductivity can also be utilized in self-regulating heaters to protect electronic devices from irreversible damage in the event of overheating by efficiently trapping the heat and giving quick feedback to the protecting system.^[55] It can be also used in thermal barrier coating of wearable devices, in which the Joule heat needs to be prevented from flowing through the device to burn skin meanwhile efficiently spreading out (along the in-plane direction) to prevent overheating of the devices.

3. Conclusions

In conclusion, we measured the anisotropic thermal conductivity of single-crystalline HfTe₅, for the first time, using the TDTR and beam-offset methods. The thermal conductivity values along *a*, *b*, and *c* axes are obtained as 11.3 ± 2.2, 0.41 ± 0.04, and 3.2 ± 2.0 W m⁻¹ K⁻¹, respectively, with a large anisotropy ratio of 28:1:8. We find that they are higher than those of ZrTe₅, thus providing a critical revisit to the prevailing knowledge in the literature that HfTe₅ has lower thermal conductivity. By using DFT calculations, we have identified the origin of the unusually higher thermal conductivities in HfTe₅ to be the longer acoustic-phonon relaxation times, owing to the weaker anharmonicity. We notice that this phenomenon, i.e., heavier compound has weaker anharmonicity and longer relaxation time than lighter ones with the same structure, is also seen in some other chalcogenides. The present work provides fundamental understanding of thermal transport in transition-metal pentatellurides, which show promise for applications in directional thermal management.

4. Experimental Section

Sample Preparation: HfTe₅ single crystals were synthesized using the chemical vapor transport (CVT) method, with iodine as the transport agency. Stoichiometric amounts of Hf(3N) and Te(5N) powders, together with 5 mg mL⁻¹ I₂, were loaded into a quartz tube under argon atmosphere. The quartz tube was flame-sealed under dynamic vacuum and then placed into a two-zone furnace, and a temperature gradient from 500 to 400 °C was then applied. After four weeks reaction, ribbon-shaped single crystals were obtained. The typical size was about 0.2 × 0.2 × 3 mm.

Thermal Measurements: Prior to TDTR measurements, each sample was coated with an aluminum (Al) layer of ≈50 nm by rf sputtering to serve as a metal transducer. A SiO₂ reference sample was also coated with the Al transducer in the same batch along with each HfTe₅ sample. The thermal conductivity of Al (59 ± 3 W m⁻¹ K⁻¹) was determined from thermal measurements of the reference SiO₂ sample with known thermophysical properties

Table 2. Comparison of the long-wavelength through-plane LA phonon velocities and thermal conductivities of various representative layered crystals. The values without references are calculated using DFT in this work.

	HfTe ₅	ZrTe ₅	Graphite	Bi ₂ Te ₃	BP	MoS ₂	MoSe ₂	WSe ₂	SnSe
ν_{sound} (km s ⁻¹)	2.13	2.14	4.34 ^[50]	3.29	4.63	3.67 ^[51]	2.93 ^[52]	2.90 ^[52]	3.45
κ_{\perp} (W m ⁻¹ K ⁻¹)	0.41	0.33 ^[19]	6.8 ^[53]	0.8 ^[54]	5.8 ^[32]	2.1 ^[51]	5.5 ^[52]	6.5 ^[52]	0.47 ^[20]

($1.35 \text{ W m}^{-1} \text{ K}^{-1}$) as done previously.^[32] As a cross check, the thermal conductivity of the Al transducer ($57 \pm 3 \text{ W m}^{-1} \text{ K}^{-1}$) converted from its electrical conductivity measured with the four-point probe method, based on the Wiedemann–Franz law, was also obtained. The values of Al thermal conductivity obtained from the two approaches agreed well. The thickness of the Al layer was determined using picosecond acoustics.^[34,56] The values of heat capacity for Al and HfTe₅ crystals were taken from the literature.^[57,58]

In TDTR measurements of the through-plane thermal conductivity, a 5× objective lens was used to produce a spot size of $w_0 \approx 12 \mu\text{m}$. The in-phase (V_{in}) and out-of-phase (V_{out}) signals were collected by a photodetector and then sent via an rf lock-in amplifier to a computer for further data analysis. For each sample, TDTR measurements were conducted at three modulation frequencies (1.6, 9, and 18 MHz) and its thermal conductivity was obtained by simultaneously fitting three sets of TDTR data (ratio of signal, $-V_{\text{in}}/V_{\text{out}}$) to a thermal diffusion model.^[36] In the beam-offset measurements of the in-plane thermal conductivity, a 20× objective lens was used to produce a much smaller beam spot ($1/e^2$ radius of $w_0 \approx 2.8 \mu\text{m}$). A delay time of -50 ps and a modulation frequency of 1.6 MHz were used to maximize the measurement sensitivity to the in-plane thermal conductivities of HfTe₅. The final results of through-plane and in-plane thermal conductivities were averaged over four to eight different locations on different samples.

DFT Calculations: The phonon dispersion relation was calculated using Phonopy^[59] and a finite difference method for a supercell composed of $3 \times 3 \times 2$ primitive cells (216 atoms). The phonon renormalization at finite temperature was done by using the ALAMODE package.^[60,61] DFT calculations were performed using the Vienna Ab initio Simulation Package (VASP)^[62] using the local density approximation (LDA) for exchange and correlation and the projector-augmented-wave method.^[63] As discussed in the introduction and following the work by Zhu et al.,^[19] vdW functionals were not included. The plane-wave energy cutoff was 500 eV. The energy convergence threshold was set at 10^{-8} eV . In the cell relaxation, the force convergence threshold was $10^{-7} \text{ eV \AA}^{-1}$, and the relaxed lattice constants for conventional unit cell, converted from two primitive cells, were $a = 3.9131$, $b = 14.254$, and $c = 13.505 \text{ \AA}$, which agree well with the experimental values^[64] $a = 3.9713$, $b = 14.499$, and $c = 13.729 \text{ \AA}$ at room temperature and $a = 3.9640$, $b = 14.443$, and $c = 13.684 \text{ \AA}$ at 10 K. It was noted that the inclusion of vdW functionals cannot give a better lattice constant. The phonon relaxation time was calculated using perturbation theory with the third-order force constants obtained using Thirddorder^[65] in $3 \times 3 \times 1$ primitive cells (108 atoms) considering up to the sixth nearest neighbor. The thermal conductivity was calculated using a $14 \times 14 \times 6$ q-mesh.

Supporting Information

Supporting Information is available from the Wiley Online Library or from the author.

Acknowledgements

T.F. and X.W. contributed equally to this work. Theoretical work at Vanderbilt University was supported by the Department of Energy grant DE-FG0209ER46554 and by the McMinn Endowment. Computations were performed at the National Energy Research Scientific Computing Center (NERSC), a Department of Energy, Office of Science, User Facility funded through Contract No. DE-AC02-05CH11231. Computations also used the Extreme Science and Engineering Discovery Environment (XSEDE). TDTR measurements were supported by the National Science Foundation (NSF award No. 1804840) and partially by the Institute on the Environment. Parts of this work were carried out in the Characterization Facility, University of Minnesota, which is partially supported by the National Science Foundation through the University of Minnesota MRSEC under Award

Number DMR-1420013. Sample preparation was conducted in the Minnesota Nano Center, which is supported by the NSF through the National Nano Coordinated Infrastructure Network (NNCI No. ECCS-1542202). Sample synthesis was conducted by P.P.W., L.Y.Z., and X.D. with the supports from Guangdong Innovative and Entrepreneurial Research Team Program (No.2016ZT06D348), NFSC (11874193), and the Shenzhen Fundamental subject research Program (JCYJ20170817110751776) and (JCYJ20170307105434022).

Conflict of Interest

The authors declare no conflict of interest.

Keywords

pentatellurides, phonons, thermal conductivities, time-domain thermoreflectance

Received: September 3, 2019

Revised: October 23, 2019

Published online: December 9, 2019

- [1] F. DiSalvo, R. Fleming, J. Waszczak, *Phys. Rev. B* **1981**, *24*, 2935.
- [2] S. Okada, T. Sambongi, M. Ido, *J. Phys. Soc. Jpn.* **1980**, *49*, 839.
- [3] E. Skelton, T. Wieting, S. Wolf, W. Fuller, D. U. Gubser, T. Francavilla, F. Levy, *Solid State Commun.* **1982**, *42*, 1.
- [4] S. Okada, T. Sambongi, M. Ido, Y. Tazuke, R. Aoki, O. Fujita, *J. Phys. Soc. Jpn.* **1982**, *51*, 460.
- [5] M. Rubinstein, *Phys. Rev. B* **1999**, *60*, 1627.
- [6] P. Shahi, D. J. Singh, J. P. Sun, L. X. Zhao, G. F. Chen, Y. Y. Lv, J. Li, J.-Q. Yan, D. G. Mandrus, J.-G. Cheng, *Phys. Rev. X* **2018**, *8*, 021055.
- [7] D. McIlroy, S. Moore, D. Zhang, J. Wharton, B. Kempton, R. Littleton, M. Wilson, T. Tritt, C. Olson, *J. Phys.: Condens. Matter* **2004**, *16*, L359.
- [8] G. Manzoni, A. Sterzi, A. Crepaldi, M. Diego, F. Cilento, M. Zacchigna, P. Bugnon, H. Berger, A. Magrez, M. Gironi, F. Parmigiani, *Phys. Rev. Lett.* **2015**, *115*, 207402.
- [9] H. Weng, X. Dai, Z. Fang, *Phys. Rev. X* **2014**, *4*, 011002.
- [10] R. Chen, Z. Chen, X.-Y. Song, J. Schneeloch, G. Gu, F. Wang, N. Wang, *Phys. Rev. Lett.* **2015**, *115*, 176404.
- [11] X.-B. Li, W.-K. Huang, Y.-Y. Lv, K.-W. Zhang, C.-L. Yang, B.-B. Zhang, Y. Chen, S.-H. Yao, J. Zhou, M.-H. Lu, L. Sheng, S.-C. Li, J.-F. Jia, Q.-K. Xue, Y.-F. Chen, D.-Y. Xing, *Phys. Rev. Lett.* **2016**, *116*, 176803.
- [12] Y. Zhang, C. Wang, L. Yu, G. Liu, A. Liang, J. Huang, S. Nie, X. Sun, Y. Zhang, B. Shen, J. Liu, H. Weng, L. Zhao, G. Chen, X. Jia, C. Hu, Y. Ding, W. Zhao, Q. Gao, C. Li, S. He, L. Zhao, F. Zhang, S. Zhang, F. Yang, Z. Wang, Q. Peng, X. Dai, Z. Fang, Z. Xu, *Nat. Commun.* **2017**, *8*, 15512.
- [13] Q. Li, D. E. Kharzeev, C. Zhang, Y. Huang, I. Pletikosić, A. Fedorov, R. Zhong, J. Schneeloch, G. Gu, T. Valla, *Nat. Phys.* **2016**, *12*, 550.
- [14] Y. Zhou, J. Wu, W. Ning, N. Li, Y. Du, X. Chen, R. Zhang, Z. Chi, X. Wang, X. Zhu, P. Lu, C. Ji, X. Wan, Z. Yang, J. Sun, W. Yang, M. Tian, Y. Zhang, H.-k. Mao, *Proc. Natl. Acad. Sci. USA* **2016**, *113*, 2904.
- [15] Y. Qi, W. Shi, P. G. Naumov, N. Kumar, W. Schnelle, O. Barkalov, C. Shekhar, H. Borrmann, C. Felser, B. Yan, S. A. Medvedev, *Phys. Rev. B* **2016**, *94*, 054517.
- [16] F. Tang, Y. Ren, P. Wang, R. Zhong, J. Schneeloch, S. A. Yang, K. Yang, P. A. Lee, G. Gu, Z. Qiao, L. Zhang, *Nature* **2019**, *569*, 537.
- [17] S. A. Miller, I. Witting, U. Aydemir, L. Peng, A. J. Rettie, P. Gorai, D. Y. Chung, M. G. Kanatzidis, M. Grayson, V. Stevanović, E. S. Toberer, G. J. Snyder, *Phys. Rev. Appl.* **2018**, *9*, 014025.
- [18] M. Hooda, C. Yadav, *Appl. Phys. Lett.* **2017**, *111*, 053902.

- [19] J. Zhu, T. Feng, S. Mills, P. Wang, X. Wu, L. Zhang, S. T. Pantelides, X. Du, X. Wang, *ACS Appl. Mater. Interfaces* **2018**, *10*, 40740.
- [20] L.-D. Zhao, S.-H. Lo, Y. Zhang, H. Sun, G. Tan, C. Uher, C. Wolverton, V. P. Dravid, M. G. Kanatzidis, *Nature* **2014**, *508*, 373.
- [21] B. Zawilski, R. Littleton IV, T. M. Tritt, *Appl. Phys. Lett.* **2000**, *77*, 2319.
- [22] C. Wang, H. Wang, Y. Chen, S.-H. Yao, J. Zhou, *J. Appl. Phys.* **2018**, *123*, 175104.
- [23] P. Gorai, E. S. Toberer, V. Stevanović, *J. Mater. Chem. A* **2016**, *4*, 11110.
- [24] O. Hellman, D. A. Broido, *Phys. Rev. B* **2014**, *90*, 134309.
- [25] G. Fugallo, A. Cepellotti, L. Paulatto, M. Lazzeri, N. Marzari, F. Mauri, *Nano Lett.* **2014**, *14*, 6109.
- [26] Y. Kuang, L. Lindsay, B. Huang, *Nano Lett.* **2015**, *15*, 6121.
- [27] T. Feng, X. Ruan, *Phys. Rev. B* **2016**, *93*, 045202.
- [28] T. Feng, L. Lindsay, X. Ruan, *Phys. Rev. B* **2017**, *96*, 161201.
- [29] T. Feng, X. Ruan, *Phys. Rev. B* **2018**, *97*, 045202.
- [30] J. Zhu, X. Wu, D. M. Lattery, W. Zheng, X. Wang, *Nanoscale Microscale Thermophys. Eng.* **2017**, *21*, 177.
- [31] J. Zhu, Y. Zhu, X. Wu, H. Song, Y. Zhang, X. Wang, *Appl. Phys. Lett.* **2016**, *108*, 231903.
- [32] J. Zhu, H. Park, J.-Y. Chen, X. Gu, H. Zhang, S. Karthikeyan, N. Wendel, S. A. Campbell, M. Dawber, X. Du, M. Li, J.-P. Wang, R. Yang, X. Wang, *Adv. Electron. Mater.* **2016**, *2*, 1600040.
- [33] X. Wu, J. Walter, T. Feng, J. Zhu, H. Zheng, J. F. Mitchell, N. Biškup, M. Varela, X. Ruan, C. Leighton, X. Wang, *Adv. Funct. Mater.* **2017**, *27*, 1704233.
- [34] G. T. Hohensee, W.-P. Hsieh, M. D. Losego, D. G. Cahill, *Rev. Sci. Instrum.* **2012**, *83*, 114902.
- [35] J. P. Feser, J. Liu, D. G. Cahill, *Rev. Sci. Instrum.* **2014**, *85*, 104903.
- [36] D. G. Cahill, *Rev. Sci. Instrum.* **2004**, *75*, 5119.
- [37] M. Omini, A. Sparavigna, *Phys. B* **1995**, *212*, 101.
- [38] D. A. Broido, M. Malorny, G. Birner, N. Mingo, D. A. Stewart, *Appl. Phys. Lett.* **2007**, *91*, 231922.
- [39] T. Feng, X. Ruan, *J. Nanomater.* **2014**, *2014*, 206370.
- [40] T. Tadano, S. Tsuneyuki, *Phys. Rev. B* **2015**, *92*, 054301.
- [41] T. M. Tritt, M. L. Wilson, R. L. Littleton, C. Feger, J. Kolis, A. Johnson, D. T. Verebelyi, S. J. Hwu, M. Fakhruddin, F. Levy, *MRS Proc.* **1997**, *478*, 249.
- [42] D. Bessas, I. Sergueev, H.-C. Wille, J. Perßon, D. Ebling, R. Hermann, *Phys. Rev. B* **2012**, *86*, 224301.
- [43] X. Chen, H. Zhou, A. Kiswandhi, I. Miotkowski, Y. Chen, P. Sharma, A. L. Sharma, M. Hekmaty, D. Smirnov, Z. Jiang, *Appl. Phys. Lett.* **2011**, *99*, 261912.
- [44] Y. Zhang, X. Ke, C. Chen, J. Yang, P. R. C. Kent, *Phys. Rev. B* **2009**, *80*, 024304.
- [45] A. H. Romero, E. K. U. Gross, M. J. Verstraete, O. Hellman, *Phys. Rev. B* **2015**, *91*, 214310.
- [46] S. Lee, K. Esfarjani, T. Luo, J. Zhou, Z. Tian, G. Chen, *Nat. Commun.* **2014**, *5*, 3525.
- [47] Y. Xia, *Appl. Phys. Lett.* **2018**, *113*, 073901.
- [48] S. Mukhopadhyay, D. S. Parker, B. C. Sales, A. A. Puretzky, M. A. McGuire, L. Lindsay, *Science* **2018**, *360*, 1455.
- [49] M. Gurvitch, *Phys. Rev. B* **1981**, *24*, 7404.
- [50] E. Hazrati, G. A. de Wijs, G. Brocks, *Phys. Rev. B* **2014**, *90*, 155448.
- [51] A. N. Gandi, U. Schwingenschlögl, *EPL* **2016**, *113*, 36002.
- [52] S. Kumar, U. Schwingenschlögl, *Chem. Mater.* **2015**, *27*, 1278.
- [53] Y. S. Touloukian, *Thermal Conductivity: Nonmetallic Solids*, IFI/Plenum, New York 1970.
- [54] C. B. Satterthwaite, R. W. Ure, *Phys. Rev.* **1957**, *108*, 1164.
- [55] Y. Wang, D. H. Hurley, E. P. Luther, M. F. Beaux II, D. R. Vodnik, R. J. Peterson, B. L. Bennett, I. O. Usov, P. Yuan, X. Wang, M. Khafizov, *Carbon* **2018**, *129*, 476.
- [56] G. L. Eesley, B. M. Clemens, C. A. Paddock, *Appl. Phys. Lett.* **1987**, *50*, 717.
- [57] D. Ditmars, C. Plint, R. Shukla, *Int. J. Thermophys.* **1985**, *6*, 499.
- [58] R. Shaviv, E. F. Westrum, H. Fjellvåg, A. Kjekshus, *J. Solid State Chem.* **1989**, *81*, 103.
- [59] A. Togo, I. Tanaka, *Scr. Mater.* **2015**, *108*, 1.
- [60] T. Tadano, Y. Gohda, S. Tsuneyuki, *J. Phys.: Condens. Matter* **2014**, *26*, 225402.
- [61] T. Tadano, S. Tsuneyuki, *Phys. Rev. B* **2015**, *92*, 054301.
- [62] G. Kresse, J. Hafner, *Phys. Rev. B* **1993**, *47*, 558.
- [63] G. Kresse, D. Joubert, *Phys. Rev. B* **1999**, *59*, 1758.
- [64] H. Fjellvåg, A. Kjekshus, *Solid State Commun.* **1986**, *60*, 91.
- [65] W. Li, J. Carrete, N. A. Katcho, N. Mingo, *Comput. Phys. Commun.* **2014**, *185*, 1747.